Annals of the BMVA Vol. 2012, No. 8, pp 1–15 (2012)

A bottom-up approach for the analysis of haustral fold ridges in CTC-CAD

Tahir Nawaz[1] and Greg Slabaugh[2]

[1]School of Electronic Engineering and Computer Science,
Queen Mary University of London,
London, United Kingdom
[2]Department of Computing,
City University London,
London, United Kingdom
⟨tahir.nawaz@eecs.qmul.ac.uk,gregory.slabaugh.1@city.ac.uk⟩

Abstract

Computer Aided Detection (CAD) systems assist radiologists in the detection of colorectal lesions. The performance of CAD systems, however, suffers due to the presence of false positives (FPs) which are introduced by various sources. One of the main sources of FPs in CAD systems is haustral folds. This paper presents a new bottom-up data-driven method to analyse and detect haustral folds. The existing methods, which are mostly based on local differential geometric computations, can be particularly unreliable to detect thicker folds. Instead, the proposed method builds a local-to-global model of the fold ridge and analyses folds on a much larger scale. We also introduce the *density of ridge candidates* (DRC), a novel geometric feature, which can effectively reduce CAD false positives. The effectiveness of the proposed method is demonstrated on a challenging dataset of 333 CAD marks. These CAD marks were detected on a data from 34 patients using a CAD system presented in [Slabaugh et al., 2010]. Our results show an encouraging **14.13%** FP reduction without the loss of any sensitivity.

1 Introduction

Colon cancer detection has been a well-researched area [Yoshida and Näppi, 2001, Huang et al., 2005, Lamy and Summers, 2007, Umemoto et al., 2008, Chowdhury et al., 2009, Lawrence et al., 2010, van Wijk et al., 2010, Epstein et al., 2010] as it is one of the leading causes of cancer deaths in developed countries [Potter et al., 1993]. This highlights the need of a timely screening and detection of pre-cancerous polyps as it can significantly reduce chances of colon cancer [Winawer, 2006]. Optical Colonoscopy (OC) is a standard procedure for the diagnosis of colorectal lesions; however, its disadvantages including invasiveness, difficulties

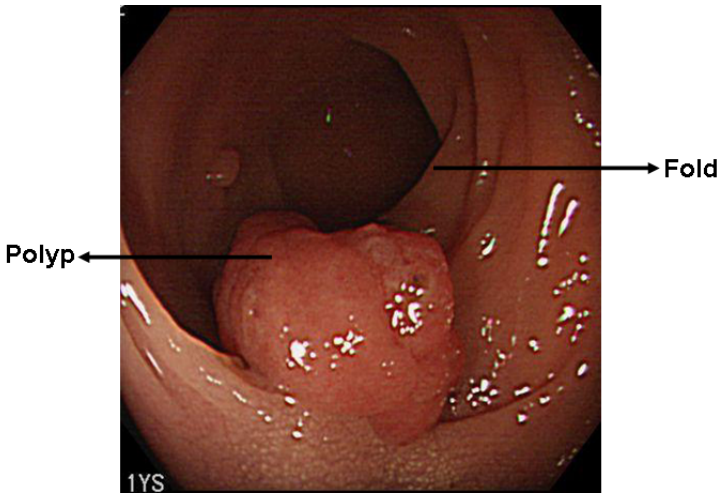

Figure 1: Endoscopic view of colon containing a polyp. Both haustral folds and polyps are protrusions on the colon surface.

in imaging the entire colon, use of sedation, and risk of perforation, present some challenges. An alternative is CT Colonography (CTC) in which a radiologist examines CT images of a colon, whose preparation involves cleansing and insufflation, as well as visualisation software to detect colon polyps. The accuracy of CTC, however, depends on the skill level of the radiologist. Further, after reading several cases, fatigued radiologists may have diminished their performance in detecting lesions. Computer Aided Detection (CAD) systems [van Wijk et al., 2010, Slabaugh et al., 2010] are developed using image processing and pattern recognition algorithms to assist radiologists in the analysis of CT data and automatically detect the possibly missed lesions. The performance of CAD systems is affected due to the presence of false positives (FPs) introduced by various sources [Lawrence et al., 2010, Slabaugh et al., 2010]. One of the leading sources of FPs is haustral folds [Lawrence et al., 2010, van Wijk et al., 2010] which is because both haustral folds and polyps are protruded entities on the colon surface when viewed endoluminally (Fig. 1), and sometimes, it becomes difficult for CAD to distinguish between them. Therefore, detection of haustral folds can help to remove FPs which will result in the improvement of CAD performance. In addition to the use of haustral fold detection to remove FPs, it is also useful in other CTC applications. For example, [Oda et al., 2009] presented a haustral fold detection method to register CT images taken from prone and supine positions. Similarly, [Roth et al., 2011] also introduced an algorithm for prone-supine registration, which was largely based on matching folds. Additionally, [Lamy and Summers, 2007] employed the detection of haustral folds to detect teniae coli.

1.1 Related work

In this section, we present a review of the previous work related to the detection of haustral folds. Yoshida and Näppi [Yoshida and Näppi, 2001] presented a CAD method which distinguished between true positives (colonic polyps) and false positives (including folds) based on the voxel-level computations of 3D geometric features (shape index and curvedness) and achieved a further reduction of system false positives using 3D volumetric features (gradient concentration and directional gradient concentration).

Huang et al. [Huang et al., 2005] proposed a method to detect folds by estimating surface curvatures. They developed a two-step method which was a hybrid of patch fitting methods. With their hybrid patch-based methods, they demonstrated a reduction in false positives (including folds) in CTC-CAD.

Lamy and Summers [Lamy and Summers, 2007] presented a haustral fold detection method which involved first generating fold candidates by creating connected components based on the local estimation of principal curvatures on the surface mesh and then applying morphological operations to further refine them. The decision of whether a connected component is fold or not is then made based on geometric filtering.

Umemoto et al. [Umemoto et al., 2008] introduced a method which also used estimation of curvatures on the colonic wall to detect folds and then used that information to extract the teniae coli. Oda et al. [Oda et al., 2008] proposed a haustral fold detection method which was based upon eigenvalues of the Hessian matrix. Moreover, a difference filter was proposed in [Oda et al., 2009] which computed the difference of CT values along the centerline of colon and used it to detect folds.

Chowdhury et al. [Chowdhury et al., 2009] proposed two methods for haustral fold detection. While the first method was based on a level sets approach applied on the extracted mesh of the colon surface, the second method combined heat diffusion and fuzzy c-means algorithm to detect folds in colon volume. Since the former tends to under-segment and the latter tends to over-segment folds, an approach was later presented in [Chowdhury et al., 2010] which combined both methods to improve the fold detection performance.

Recently, Wei et al. [Wei et al., 2010] presented an approach which employed image processing operations on the transformed 2D surface of colon to detect haustral folds. Their method involved extraction of features from 2D flattened surface of colon by applying 2D Gabor filters followed by edge detection using Sobel operator and thresholding to yield folds.

1.2 Contributions

Previous solutions for haustral fold detection rely primarily on local computations around a voxel in the image or a mesh vertex, typically of the order of $1-2mm$ of resolution. However, folds are elongated objects that are significantly larger, often having lengths in the range of $20-50mm$. In this paper, we demonstrate the advantage of our bottom-up approach that globally analyses folds at this scale. We model the fold ridge geometrically, from which we derive a novel feature, the *density of ridge candidates* (DRC), that is shown to be highly effective in reducing FPs in CAD system. Unlike [Zhu et al., 2010] which employed the ridge-line detection for the segmentation of folds, the proposed method is aimed more towards the analysis of folds, and additionally, it can filter out FPs significantly with no impact on the sensitivity. Unlike another method [Lindeberg, 1998] which used intensity-based local differential computations to detect ridges in a 2D image, the proposed method detects ridge on the extracted meshes due to reasons discussed in Sec. 2.2. An initial version of this work appeared in [Nawaz and Slabaugh, 2011]. Unlike [Nawaz and Slabaugh, 2011], this paper provides a more detailed analysis and validation of the proposed method. Moreover, we also demonstrate the effectiveness of the proposed method by showing a significant improvement in terms of FP reduction as compared to a local differential computation-based approach.

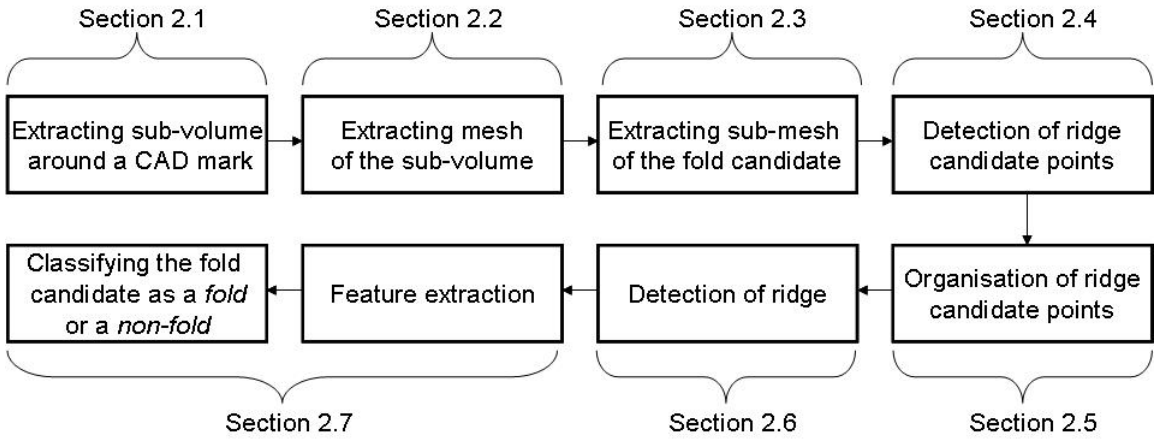

Figure 2: Block diagram of the proposed haustral fold analysis and detection method

The rest of the paper is organised as follows. Section 2 presents a step-by-step description of the proposed haustral fold analysis and detection method. Section 3 describes the experimental analysis and results. The paper is concluded in Sec. 4 while giving direction of the future work in Sec. 5.

2 Proposed haustral fold analysis and detection method

Figure 2 shows the block diagram of the proposed haustral fold analysis and detection method. Below is given a description of each block of the proposed method.

2.1 Extracting sub-volume around a CAD mark

Given a CAD mark, a detected polyp location (a point) in the CT volume, the method first extracts a $50mm^3$ sub-volume around it. Figure 3 shows examples of some CT slices with CAD marks indicated as red circles. In the experimentation, we used a set of 333 CAD marks detected using the CAD system presented in [Slabaugh et al., 2010] on a data from 34 patients. The extracted sub-volume of a CAD mark is used for further processing in the following steps of the proposed method.

2.2 Extracting mesh of the sub-volume

We apply the marching cubes algorithm [Lorensen and Cline, 1987] to the extracted image sub-volume to obtain a triangular mesh. In this regard, we use a threshold of -800 (in Hounsfield units) which selects the voxels (cubes) that contribute to the formation of the mesh. The values of the CT image are normalised in Hounsfield Units (HU). In HU, voxels corresponding to air have a value of -1000, to water have a value of 0, and to bone have a value of 1000. The threshold of -800 is absolute to the Hounsfield unit scale and represents an iso-intensity level between air and tissue. Such a value is common in iso-surface extraction in CT image, for example, see [Summers et al., 2005].

We work with the triangular mesh for two reasons. First, since the folds are outward (when viewed endoluminally) protrusions of the colon surface, the change in their shape

(a) (b) (c)

Figure 3: Examples of some CT slices. CAD mark locations are shown as red circles. (a) An example of a true positive (TP) CAD mark located at $(247, 246, 143)$ in the CT slice; (b) an example of a false positive (FP) CAD mark located at $(142, 209, 286)$ in the CT slice; (c) an example of a false positive (FP) CAD mark located at $(88, 262, 248)$ in the CT slice.

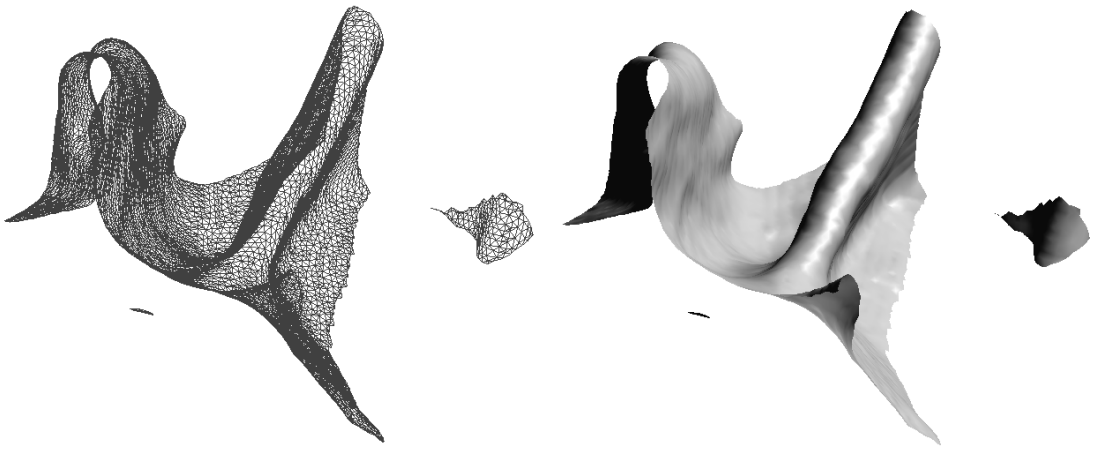

(a) (b)

Figure 4: Visualisation of an extracted mesh of a sub-volume (a) and its solid rendering (b).

can easily be studied on a two dimensional manifold rather than the 3D volumetric CT data [Lamy and Summers, 2007]. Secondly, recent studies have shown that it is more accurate to compute surface curvatures on mesh than on the volumetric data [Sundaram, 2008]. A visualisation of extracted mesh of a sub-volume is given in Fig. 4(a), Fig. 4(b).

2.3 Extracting sub-mesh of fold candidate

Inspired by [Li et al., 2009], for each vertex $\mathbf{v}$ of the mesh, the average distance of points in the 2-ring neighbourhood of $\mathbf{v}$ from the plane running through $\mathbf{v}$ and orthogonal to its surface normal $\hat{c}$ is computed (Fig. 5(a)). The distance is large where the mesh is curved, and low where the mesh is locally flat. Hysteresis thresholding is applied to this distance,

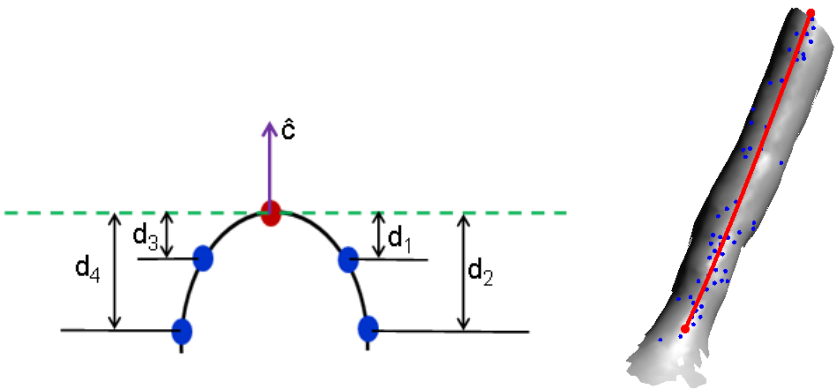

(a) (b)

Figure 5: (a) Extraction of sub-mesh of fold candidates is inspired from [Li et al., 2009] which involves computing the average of distances (d_1, d_2, d_3, d_4) of points (shown in blue) that are in the 2-ring neighbourhood of the vertex under consideration $\mathbf{v}$ (shown in red) from the plane (shown as green broken line) running through $\mathbf{v}$ and orthogonal to its surface normal $\hat{c}$. The larger the average distance, the more curved is the mesh and vice versa. (b) Example of a sub-mesh extracted from the mesh is shown in Fig. 4. The blue points on it are the detected ridge candidate points and the red line is the detected ridge of the fold.

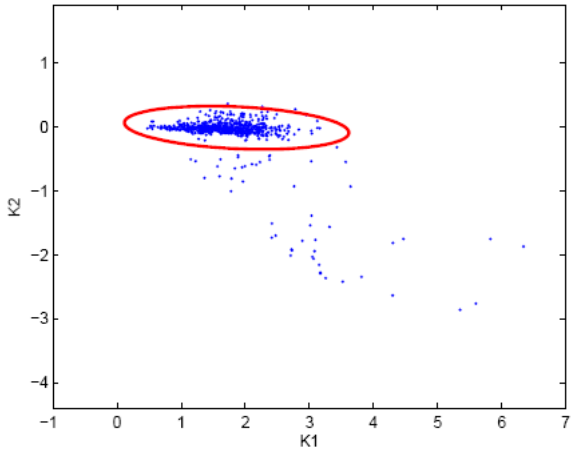

Figure 6: Distribution of K_1 and K_2 computed on annotated ridge candidate points. The outliers have been filtered out and the resulting distribution is fitted into a 2D Gaussian.

producing fold candidates, and the one closest to the CAD mark is retained. In hysteresis thresholding, the choice of the lower threshold τ_{lower} is discussed in Sec. 3, and the upper threshold is computed adaptively and is explained as follows. The largest average distance value among that of all the vertices which are less than five voxels away from the CAD mark is chosen as the upper threshold. This produces a smaller region of interest (sub-mesh) containing only the raised portion of the mesh (either the fold or polyp) closest to the given CAD mark. Figure 5(b) shows an example of a sub-mesh extracted (with $\tau_{lower} = 0.07$) from the mesh shown in Fig. 4.

Annals of the BMVA Vol. 2012, No. 8, pp 1–15 (2012)

2.4 Detection of ridge candidate points

To detect ridge candidate points on a fold candidate, a data-driven probabilistic model of the fold ridge is created by analysing the behaviour of principal curvatures (K_1 and K_2), computed on the mesh using the Gauss-Bonnet scheme described in [Magid et al., 2007], on real fold ridges. We manually annotated 732 points on 17 fold ridges, and plotted their corresponding principal curvature values as shown in Fig. 6. From this figure, it is clear that K_1 tends to be positive and K_2 is nearly zero for most of the points, which corresponds to our intuition since points on the fold ridge tend to be locally cylindrical in shape. There are some outliers in Fig. 6 which are possibly caused due to some annotations on *non-ridge* areas of the selected fold sub-meshes. To minimise the effect of outliers in the model, they have been filtered out and the resulting distribution is fitted into a 2D Gaussian and is given by:

$$P(K_1, K_2) = exp\left\{\frac{-1}{2(1-\rho^2)}\left[\left(\frac{K_1 - m_1}{\sigma_1}\right)^2 - 2\rho\left(\frac{K_1 - m_1}{\sigma_1}\right)\left(\frac{K_2 - m_2}{\sigma_2}\right) + \left(\frac{K_2 - m_2}{\sigma_2}\right)^2\right]\right\}, \quad (1)$$

where $P(K_1, K_2)$ represents the probability of a mesh vertex to be a ridge candidate point given its K_1 and K_2, $(m_1, m_2) = (1.6787, -0.0175)$ is the mean point of the 2D Gaussian distribution, σ_1 and σ_2 are the standard deviations of K_1 and K_2 respectively, ρ is the correlation coefficient of K_1 and K_2, and the computed $Covariance = \begin{bmatrix} 0.2163 & -0.0023 \\ -0.0023 & 0.0063 \end{bmatrix}$. The vertices with $P(K_1, K_2) > \tau$ are considered as ridge candidate points. The choice of τ is discussed in Sec. 3. Figure 5(b) shows a visualisation of detected ridge candidate points on an extracted fold candidate with $\tau_{lower} = 0.07$ and $\tau = 0.3$.

Ridge candidates points are unorganised 3D points. They are first organised and then fitted into a quadratic space curve to obtain the ridge.

2.5 Organisation of ridge candidate points

We adopted a three-step strategy to organise the ridge candidate points. First, we find the *start point* and *end point* of ridge based upon the Seeded Distance Transform (see [Fabbri et al., 2008] for a survey on distance transform algorithms). To find the start point, a ridge candidate point is randomly selected as a seed and Seeded Distance Transform is applied on the mesh. It assigns a distance value to all other points depending upon their geodesic distance from the seed point. The farthest point from the seed is selected as the *start point*, as it lies at one end of the ridge. Then, we repeat the same procedure again, selecting the *start point* as a seed now, to get the end point that lies at the other end of the ridge. Second, the geodesic path between the start and the end points is computed based upon A* algorithm. Third, all the points are organised based on their interpolated distance values along the geodesic path. In this regard, a point is projected on the geodesic path (closest projection is taken) and a distance value is interpolated between the distance values of the nearest two points.

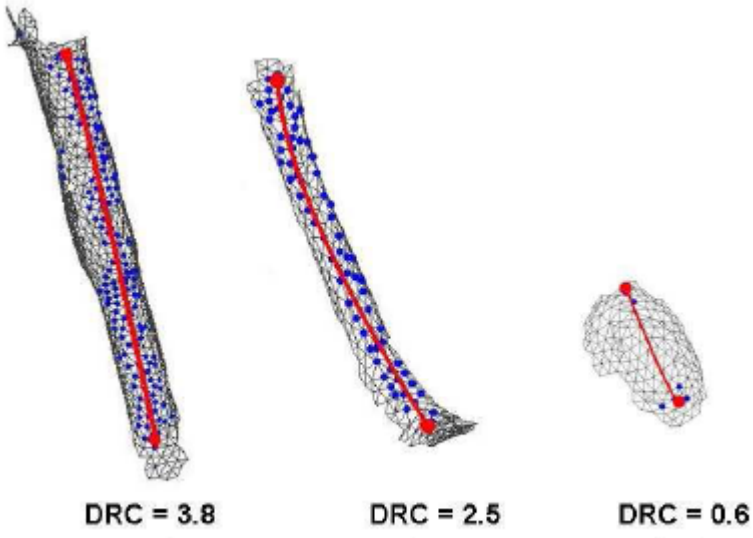

Figure 7: Examples of detected ridges. Ridge candidate points are shown in blue and ridges are shown in red colour. Left and middle sub-meshes are haustral folds as their DRC is higher, and the right sub-mesh is a polyp as its DRC is comparatively smaller.

2.6 Ridge Detection

After the organisation of ridge candidate points, they are fitted using a least squares solution, to a quadratic space curve (Eq. (2)) to obtain the geometric ridge model. The equation of the space curve is given as:

$$\mathbf{b}(t) = \mathbf{a}_0 + t\mathbf{a}_1 + t^2\mathbf{a}_2. \tag{2}$$

Writing Eq. 2 in matrix form and solving it in least square sense for N organised 3D ridge candidate points, we get:

$$\begin{bmatrix} b_x(t_0) & b_y(t_0) & b_z(t_0) \\ b_x(t_1) & b_y(t_1) & b_z(t_1) \\ \vdots & \vdots & \vdots \\ b_x(t_N) & b_y(t_N) & b_z(t_N) \end{bmatrix} = \begin{bmatrix} 1 & t_0 & t_0^2 \\ 1 & t_1 & t_1^2 \\ \vdots & \vdots & \vdots \\ 1 & t_N & t_N^2 \end{bmatrix} \begin{bmatrix} a_{0x} & a_{0y} & a_{0z} \\ a_{1x} & a_{1y} & a_{1z} \\ a_{2x} & a_{2y} & a_{2z} \end{bmatrix} \tag{3}$$

$$B = \mathcal{T}A \tag{4}$$

$$A = (\mathcal{T}^T\mathcal{T})^{-1}\mathcal{T}^T B \tag{5}$$

The system of equations is sufficiently constrained for $N \geq 3$ points. Figure 5(b) and 7 shows examples of the detected ridges for some fold candidates.

2.7 Feature extraction and classification

From our ridge model, we extract two values that are combined to form our novel feature, the *density of ridge candidates* (DRC). Specifically, we determine the following.

Annals of the BMVA Vol. 2012, No. 8, pp 1–15 (2012)

- The ridge length, L_R, computed along the quadratic space curve.
- The number of ridge candidates, N_c, which is the number of mesh vertices that have a probability (corresponding to Eq. 1) greater than τ.

L_R and N_c are discriminative for fold detection. The length is discriminative as haustral folds are elongated structures typically having length greater than that of polyps. Also, a fold will have many ridge candidates as estimated from Eq. 1 compared to polyp. We define the DRC as:

$$DRC = \begin{cases} 0, & L_R < \tau_L; \\ \frac{N_c}{L_R}, & \text{otherwise;} \end{cases} \tag{6}$$

where τ_L is a threshold (fixed to 30 in this paper). DRC is a highly discriminative feature. We expect the DRC of a fold to be greater than that of a polyp and we allow all the CAD marks having smaller ridge length (by setting their DRC to zero) to pass as a true positive (TP) so as to minimise chances of misclassifying a polyp. Some examples of the DRC computed for surfaces corresponding to both folds and polyps are shown in Figure 7.

3 Experimental analysis and results

We have tested the proposed method on CAD marks containing both TPs and FPs (including folds) detected using the CAD system presented in [Slabaugh et al., 2010]. The proposed method was tested on 333 CAD marks (57 TPs and 276 FPs), corresponding to data from 34 patients, for which we have 68 volumes (each having one prone and one supine volume). The dataset is obtained from seven different institutions from around the world. TPs and FPs are determined based on gold standard annotations produced by expert radiologists. All of our data was read by three radiologists and their input was used to produce a gold standard annotation through consensus. In the following discussion, firstly, we shall present the justifications for the choice of τ_{lower} and τ, and then analyse the performance of the proposed method.

To choose the value of τ_{lower}, we studied the effect of its variation (between 0 and 1) on the classification results at 100% sensitivity (Fig. 8) while keeping $\tau = 0.3$. We chose $\tau_{lower} = 0.1$ as it maximises the classification performance. We then studied the effect of variation of τ (between 0 and 1) on the classification results at 100% sensitivity while keeping $\tau_{lower} = 0.1$ fixed (Fig. 9). Similarly, a value of $\tau = 0.22$ is selected as it maximises the classification performance. A decrease in the value of the τ leads also to the selection of those vertices as ridge candidate points that lie outside the vicinity of the ridge and an increase in the value of τ tends to discard vertices lying in the close vicinity of the ridge, both of which are undesirable.Thus, we fixed $\tau_{lower} = 0.1$ and $\tau = 0.22$ in the experimentation and the results are discussed as follows.

Figures 10 and 11 shows the the computed values of L_R and N_c for all CAD marks. TPs and FPs are the same in both of these figures and are shown in red and blue colours respectively. Using L_R alone as a feature can provide FP reduction (Fig. 10) but at the expense of some sensitivity, which infrequently results from large or long polyps. Figure 10 demonstrates that some TPs have large ridge lengths and are more likely to be misclassified as folds. That is why, we combine with L_R the N_c in the DRC formulation as it is more robust in preserving the sensitivity while reducing a significant amount of FPs (Fig. 11).

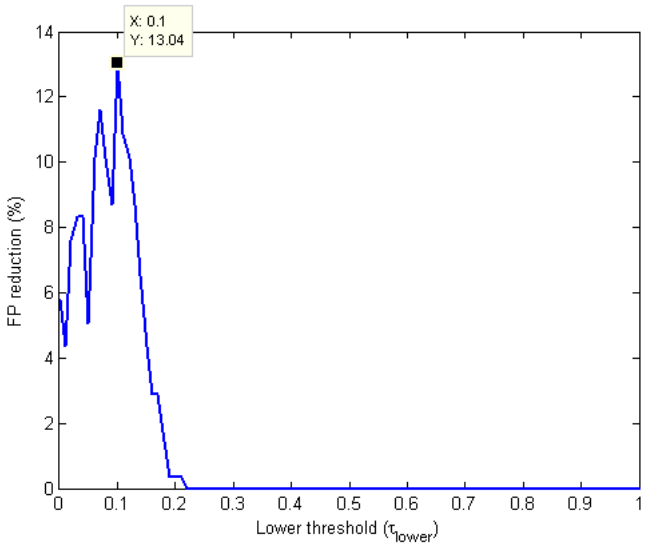

Figure 8: Selection of the lower threshold (τ_{lower}) used in hysteresis thresholding. The figure shows the effect of variation of τ_{lower} on the FP reduction at 100% sensitivity. A value of $\tau_{lower} = 0.1$ is selected as it maximises the classification performance.

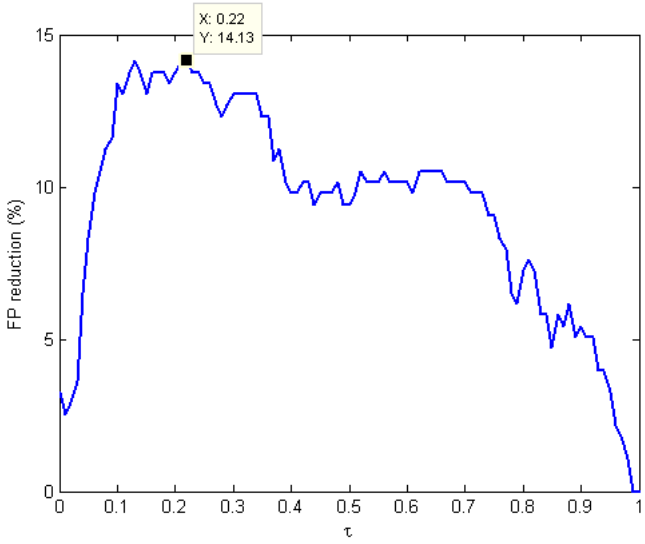

Figure 9: Selection of the value of τ. The figure shows the effect of variation of τ on the FP reduction at 100% sensitivity. A value of $\tau = 0.22$ is selected as it maximises the classification performance.

The FROC curve computed with the DRC feature is plotted in Fig. 12. The FROC curve is computed by finding the total number of FPs (divided by total volumes (68)) at all sensitivities (0 - 100%). The results are quite encouraging and a FP reduction of 14.13% is achieved with 100% sensitivity (see Fig. 12). Moreover, by moving along the FROC curve, further reduction of FPs is possible but at the expense of some sensitivity. Feedback from practic-

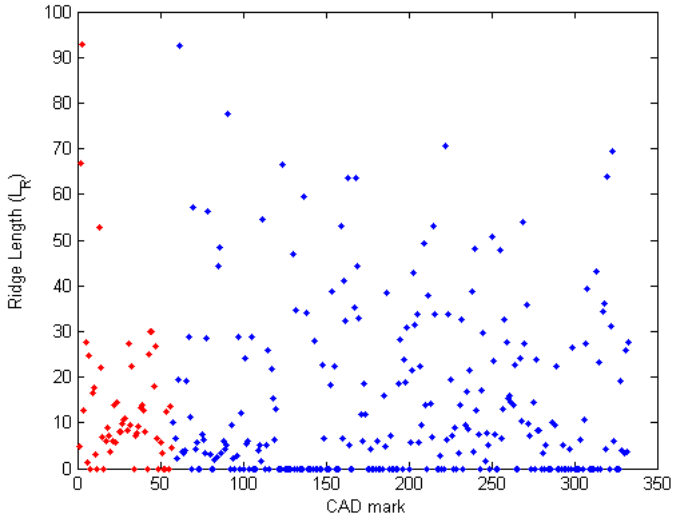

Figure 10: The computed ridge Lengths (L_R) of CAD marks. L_R is a discriminative feature and can remove FPs but at the expense of some sensitivity. On the other hand, DRC is more robust in preserving sensitivity while removing FPs (see Fig. 11). Red points are TPs and blue points are FPs. TPs and FPs are the same in this figure and Fig. 11.

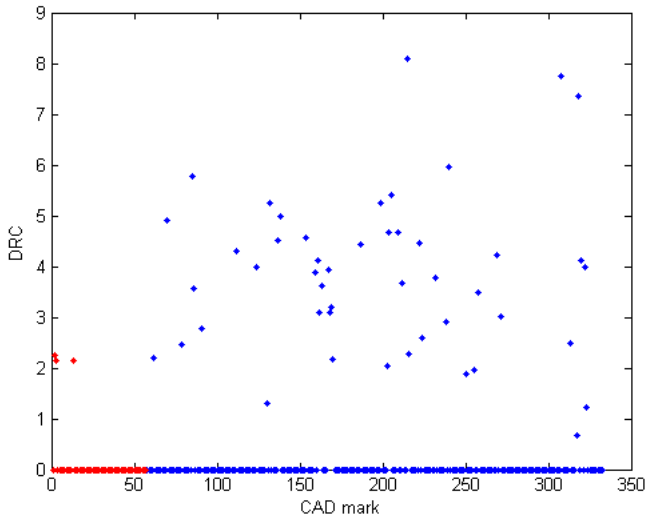

Figure 11: The computed density of ridge candidate (DRC) values of CAD marks. Unlike L_R (Fig. 10), DRC preserves sensitivity while achieving a significant FP reduction. Red points are TPs and blue points are FPs. TPs and FPs are the same in this figure and Fig. 10.

ing radiologists using CAD systems suggests that less than 5 FPs per volume is acceptable in their workflow. Of course, the fewer FPs per volume are preferred, as all CAD findings must be reviewed by the clinician. Using the proposed method, we have achieved around 3.5 FPs per volume at 100% sensitivity, and the 14.13% reduction of FPs is a considerable

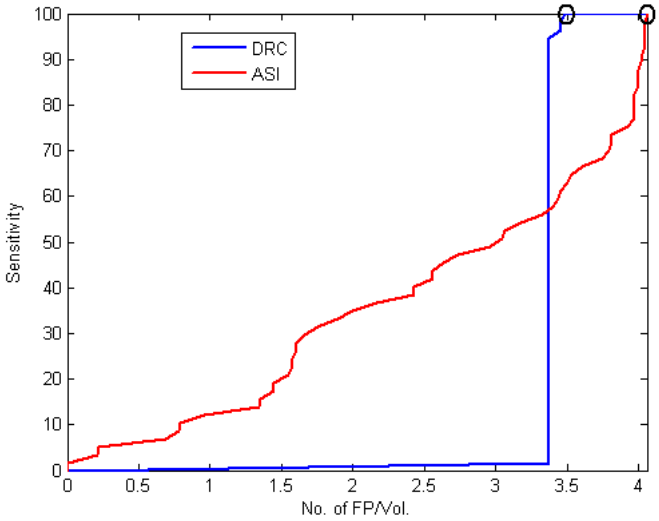

Figure 12: FROC curves computed using the DRC feature (shown in blue colour) and ASI feature (shown in red colour) with $\tau_{lower} = 0.1$ and $\tau = 0.22$. Using the DRC feature, an FP reduction of 14.13% is achieved without compromising any sensitivity (the two points used to compute the FP reduction for DRC are encircled in black colour). ASI feature, on the other hand, is not found to be robust in preserving sensitivity.

improvement and will save the clinician time in reading a case.

We also compared the performance of the proposed DRC feature with that of another feature, the *average shape index* (ASI). Epstein et al. [Epstein et al., 2010] used the shape index (SI) information in their 3D polyp segmentation framework. SI encapsulates local shape information at a point using its K_1 and K_2 values. It can be defined on a mesh vertex $\mathbf{v}$ as [Epstein et al., 2010]:

$$SI(\mathbf{v}) = \frac{1}{2} - \frac{1}{\pi} arctan \frac{K_1(\mathbf{v}) + K_2(\mathbf{v})}{K_1(\mathbf{v}) - K_2(\mathbf{v})}. \tag{7}$$

We computed ASI values for each of the 333 fold candidates and tested its classification performance. ASI of a fold candidate is computed by taking the mean of shape index values on all of its vertices. The corresponding FROC curve for ASI is shown in Fig. 12. It is clear from the results that DRC has shown superior performance in terms of FP reduction at 100% sensitivity compared to ASI (Fig. 12). The performance of ASI improves only for sensitivities lower than around 57% which is of less significance from clinical point of view. The reason of the better performance of DRC is its local-to-global formulation unlike ASI which is based on local differential computations.

The performance of the proposed method depends on how well the meshes of fold candidates are extracted, which is accurate for the majority of CAD marks in our experiments. However, in the case, where the extracted mesh of a fold candidate contains a polyp attached to a fold, DRC is found to misclassify it as a fold. This is because, in such a case, DRC value is high due to the detection of a large number of ridge candidate points N_c on the *fold-part* of the extracted mesh of the fold candidate.

4 Conclusions

In this paper, we have presented a method for haustral fold detection that can significantly reduce the false positives (FPs) in CTC-CAD. Unlike most of the existing methods that depend solely upon the *local* differential geometric computation, we have studied the haustral folds on a much larger scale. We fit a global shape model to the local detections to estimate a ridge model of haustral folds capable of robust characterisation. The overall performance of **14.13%** FP reduction with no impact on sensitivity has been demonstrated on a sufficiently large dataset of 333 CAD marks resulting from 68 CT volumes. Moreover, a comparison with a local differential computation-based approach has shown the effectiveness of the proposed method.

5 Future work

The focus of our future work is to further study the generalisation of the method so as to address the problem of misclassification of cases where polyps are attached to folds. We plan to address this problem using a *statistical shape prior* modelled with a set of example folds. From the statistical shape prior, we can compute statistical parameters (like mean and modes), and then, given a fold candidate, its extracted shape can be projected into the shape space of the model. A true fold, the one which does not have a polyp attached to it, is expected to fit better (less fitting error) than a fold with an attached polyp. Based upon this, we expect to remove the misclassified fold candidates thereby further improving the CAD performance.

It is important to highlight that the present work concentrates on the reduction of FPs produced in a CAD system without taking into account the false negatives (FNs) which may also be caused. The reduction of false negatives (FNs) is of course another important aspect of improving a CAD system. The present work is designed as an additional filter that operates on the CAD findings. If a false negative is generated by the CAD system, then it is impossible for the proposed filter to recover it, as the proposed filter is only processing the CAD findings which do not include false negatives. We are, however, interested in false negatives too, and this is a subject of other research we are undertaking.

References

A. S. Chowdhury, S. Tan, J. Yao, M. G. Linguraru, and R. M. Summers. Two methods of haustral fold detection from computed tomographic virtual colonoscopy images. In *Medical Imaging: Computer-Aided Diagnosis. Proc. of SPIE*, volume 7260, pages 72602U–1 – 72602U–8, 2009.

A. S. Chowdhury, S. Tan, J. Yao, and R. M. Summers. Colonic fold detection from computed tomographic colonography images using diffusion-FCM and level sets. *Pattern Recognition Letters*, 31(9):876–883, 2010.

M. L. Epstein, I. Sheu, and K. Suzuki. *Pattern Recognition Recent Advances*, chapter Hessian Matrix-Based Shape Extraction and Volume Growing for 3D Polyp Segmentation in CT Colonography, pages 405–418. InTech, February 2010.

R. Fabbri, L. D. F. Costa, J. C. Torelli, and O. M. Bruno. 2D euclidean distance transforms: A comparative survey. *ACM Computing Surveys*, 40(1):1–44, February 2008.

A. Huang, R. M. Summers, and A. K. Hara. Surface curvature estimation for automatic colonic polyp detection. In *Proc. of SPIE*, volume 5746, pages 393–402, 2005.

J. Lamy and R. M. Summers. Teniae coli detection from colon surface: Extraction of anatomical markers for virtual colonoscopy. In *Proc. of Int. Symposium on Visual Computing*, pages 199–207, 2007.

E. M. Lawrence, P. J. Pickhardt, D. H. Kim, and J. B. Robbins. Colorectal polyps: Stand-alone performance of computer-aided detection in a large asymptomatic screening population. *Radiology*, 256(3):791–798, 2010.

K. Li, L. Guo, J. Nie, C. Faraco, Q. Zhao, S. Miller, and T. Liu. Gyral folding pattern analysis via surface profiling. In *Proc. of Int. Conference on Medical Image Computing and Computer Assisted Intervention*, 2009.

T. Lindeberg. Edge detection and ridge detection with automatic scale selection. *Int. Journal on Computer Vision*, 30(2):117–156, 1998.

W. E. Lorensen and H. E. Cline. Marching cubes: A high resolution 3d surface construction algorithm. In *Proc. of the 14th Annual Conference on Computer Graphics and Interactive Techniques (SIGGRAPH'87)*, pages 163–169, New York, USA, July 1987.

E. Magid, O. Soldea, and E. Rivlin. A comparison of gaussian and mean curvature estimation methods on triangular meshes of range image data. *Computer Vision and Image Understanding*, 107(3):139–159, 2007.

T. Nawaz and G. Slabaugh. Global analysis of haustral fold ridges for the reduction of false positives in CTC-CAD. In *Proc. of Medical Image Understanding and Analysis*, London, July 2011.

M. Oda, T. Kitasaka, K. Mori, Y. Suenaga, T. Takayama, H. Takabatake, M. Mori, H. Natori, and S. Nawano. Haustral fold detection from 3d abdominal ct images for flat-shaped colonic polyp detection. In *Int. Journal of Computer Assisted Radiology and Surgery*, volume 3, Supplement 1, pages S188–S198, 2008.

M. Oda, T. Kitasaka, K. Mori, Y. Suenaga, T. Takayama, H. Takabatake, M. Mori, H. Natori, and S. Nawano. Haustral fold detection method for CT colonography based on difference filter along colon centerline. In *Proc. of SPIE*, volume 7260, 2009.

J. D. Potter, M. L. Slattery, R. M. Bostick, and S. M. Gapstur. Colon cancer: A review of the epidemiology. *Epidemiologic Reviews*, 15(2):499–545, 1993.

H. R. Roth, J. R. McClelland, D. J. Boone, M. Modat, M. J. Cardoso, T. E. Hampshire, M. Hu, S. Punwani, S. Ourselin, G. Slabaugh, S. Halligan, and D. J. Hawkes. Registration of the endoluminal surfaces of the colon derived from prone and supine ct colonography. *Medical Physics*, 38(8), 2011.

G. Slabaugh, X. Yang, X. Ye, R. Boyes, and G. Beddoe. A robust and fast system for CTC computer-aided detection of colorectal lesions. *Algorithms*, 3(1):21–43, 2010.

R. M. Summers, M. Franaszek, M. T. Miller, P.J. Pickhardt, J. R. Choi, and W. R. Schindler. Computer-aided detection of polyps on oral contrast-enhanced ct colonography. *American Journal of Roentgenology*, 184(1):105–108, January 2005.

P. Sundaram. *Geometry processing for colon polyp detection*. PhD thesis, Stanford University, 2008.

Y. Umemoto, M. Oda, T. Kitasaka, K. Mori, Y. Hayashi, Y. Suenaga, T. Takayama, and H. Natori. Extraction of teniae coli from CT volumes for assisting virtual colonoscopy. In *Proc. of SPIE*, volume 6916, 69160D, pages 1–10, 2008.

C. van Wijk, V. F. van Ravesteijn, F. M. Vos, and L. J. van Vliet. Detection and segmentation of colonic polyps on implicit isosurfaces by second principal curvature flow. *IEEE Trans. on Medical Imaging*, 29(3):688–698, 2010.

Z. Wei, J. Yao, S. Wang, and R. M. Summers. Haustral fold detection for ct colonography images using gabor filter. In *Proc. of Asilomar Conference on Signals, Systems and Computers*, pages 329–331, November 2010.

S. Winawer. The achievements, impact , and future of the national polyp study. *Gastrointestinal Endoscopy*, 64:975–978, 2006.

H. Yoshida and J. Näppi. Three-dimensional computer-aided diagnosis scheme for detection of colonic polyps. *IEEE Trans. on Medical Imaging*, 20(12):1261–1274, December 2001.

H. Zhu, L. Li, Y. Fan, and Z. Liang. Haustral fold segmentation of CT colonography using ridge line detection. In *Proc. of Medical Image Computing and Computer Assisted Intervention Workshop*, pages 33–39, 2010.